Journal of Electronic Materials (2023) 52:414–421
https://doi.org/10.1007/s11664-022-10002-4

ORIGINAL RESEARCH ARTICLE

Influence of Magnesium Content on the Structural, Optical, and Electrical Properties of $Cu_2(Zn_{1-x}Mg_x)SnS_4$ Nanostructured Quaternary Thin Film Synthesized Using the Sol–Gel Method

A. S. Ibraheam[1,3] · Jamal M. Rzaij[2] · M. K. Md. Arshad[3]

Received: 23 July 2022 / Accepted: 28 September 2022 / Published online: 12 October 2022

Abstract
Nanostructured Cu_2ZnSnS_4 (CZTS) and $Cu_2(Zn_{1-x}Mg_x)SnS_4$ quaternary alloys with varying magnesium (Mg) content were synthesized using a low-cost, environmentally friendly co-precipitation technique. The structural characteristics of $Cu_2(Zn_{1-x}Mg_x)SnS_4$/Si were analyzed using x-ray diffraction (XRD) and field-emission scanning electron microscopy (FE-SEM). The XRD results showed that the CZTS film crystallized the kesterite phase, whereas the Cu_2MgSnS_4 film formed a stannite phase. Increases in Mg content led to an increase in the crystallinity of the deposited alloy, and to an increase in the average crystallite size from 31.65 nm to 53.73 nm. FE-SEM micrographs indicated the morphology of more densely packed nanostructures with less porosity when the Mg content was increased, resulting in the granular structure changing to a whisker-like form. Investigation into the optical properties of photoluminescence spectra revealed a decrease in the band gap of the $Cu_2(Zn_{1-x}Mg_x)SnS_4$ film from 1.71 eV to 1.67 eV when the Mg content was increased from 0 wt.% to 1 wt.%. The current–voltage characteristics demonstrated that the prepared alloys exhibited ohmic behavior and the photocurrent improved from 1.69×10^{-4} to 2.86×10^{-4} A as the Mg content increased from 0 wt.% to 1 wt.% at an applied voltage of 6 V. The highest photosensitivity and photocurrent responsivity of the produced $Cu_2(Zn_{1-x}Mg_x)SnS_4$ quaternary alloy were 5309% and 2319%, respectively, when the Mg content was 0.7 wt.%, providing the best content for ultraviolet light detection applications.

Keywords Cu_2ZnSnS_4 · photosensitivity · quaternary alloy · sol–gel · thin film

1. Introduction

Cu_2ZnSnS_4 (CZTS) is among the most promising thin films for photovoltaic device applications because of its high absorption coefficient and low optical band gap (1.45–1.65 eV).[1–3] The maximum measured efficiency of a CZTS solar cell is 12.7%, which is less than the theoretical Shockley–Queisser limit (32.4%) and the efficiency of a Cu(In, Ga)Se_2 solar cell (22.8%).[4] The main challenge of CZTS solar cells is the open-circuit voltage deficit, defined as (Eg/q – VOC), where Eg, q, and VOC are the absorber band gap, electron charge, and open-circuit voltage, respectively.[5–7] The copper–zinc (CuZn) antisite defect is a main contributor to open-circuit voltage insufficiency induced by electrostatic potential fluctuations.[8,9] Owing to their affinity for Cu and Zn cation sizes, antisite defects are simple to create. They are predicted to limit solar cell performance and have greatly reduced the initial rapid advancement of CZTS alloys. Several theories have suggested why this is a significant band-tail effect. One of the most common reasons for the suboptimal quality of the CZTS absorber layer is the non-ideal interface and the development of secondary phases between magnesium sulfide (MgS) and CZTS.

Recent research has suggested that substituting other elements for Cu or Zn could help reduce these problems. However, the most popular alternatives, silver (Ag) and cadmium, are either scarce or poisonous, thus negating the usefulness of CZTS. Other transition metal options (e.g., iron, manganese (Mn), nickel, and cobalt) are multivalent, resulting in

✉ Jamal M. Rzaij
sc.jam72al@uoanbar.edu.iq

1 Iraqi Ministry of Education, Anbar, Iraq

2 Department of Physics, College of Science, University of Anbar, Ramadi, Iraq

3 Institute of Nano Electronic Engineering, University Malaysia Perlis, 01000 Kamgar, Perlis, Malaysia

dangerous deep-level flaws.[10,11] Mg is a prospective candidate that avoids these issues due to its abundance, innocuous nature, and stability in the + 2-oxidation state. Mg has secondary phases based on Zn, such as zinc selenide (ZnSe) and ZnS, that reduce photovoltaic performance.[12] Furthermore, Mg is naturally more abundant in the Earth's crust than Zn.[13,14]

The substitution of Zn with Mg is preferred over other elements when tuning the band gap of CZTS. Because the ionic radii of Mg and Zn are comparable, Mg^{2+} may occupy the Zn^{2+} sites in the CZTS lattice rather than segregate at the grain boundaries and the CZTS layer surface. Moreover, the addition of Mg to the CZTS absorber layer provides specific advantages in terms of cost, reserve availability, and environmental friendliness. Finally, the presence of ZnS throughout the precursor solution synthesis of CZTS may eliminate or reduce certain impurity phases. In solution, the ZnS binary phase occurs in a stable form, whereas the MgS binary phase is unstable. Therefore, substituting in Mg for Zn is a cost-effective method for adjusting the CZTS band gap.[15]

Recently, Wang et al. investigated the effect of substituting Zn with varied Mg doping ratios on the characteristics of $Cu_2Mg_xZn_{1-x}Sn(S,Se)_4$ quaternary alloy deposited using the spin-coating method with the thickness ranging from 1.78 µm to 1.80 µm.[16] The researchers concluded that the Mg content had no influence on the crystallization of the synthesized films, and that increasing the Mg content increased the energy gap and improved the electrical characteristics. Romero et al. investigated the partial and total substitution effects of Mg-substituted Zn on the structural and optical properties of the $Cu_2Zn_{1-x}Mg_xSnS_4$ quaternary semiconductor alloy deposited using the hot injection method.[17] Their structural analysis revealed the presence of secondary phases and no significant variation in the interplanar distances with increasing Mg concentration. The average size of the crystalline domains decreased at high Mg incorporation ratios, whereas the energy gap increased.

This study aims to synthesize $Cu_2Zn_{1-x}Mg_xSnS_4$ thin films with various Mg contents using a low-cost and environmentally friendly co-precipitation method. The crystal structure and electro-optic performance of the $Cu_2(Zn_{1-x}Mg_x)SnS_4$ films have been investigated. In addition, using current–voltage (*I–V*) characterization, we enhanced the electrical properties of Ag/$Cu_2(Zn_{1-x}Mg_x)SnS_4$/Ag/n-Si films with varying Mg wt.% content for photosensitivity applications.

2. Experimental

2.1 Synthesis of Deposition Solutions

A low-cost and environmentally friendly co-precipitation method was used to synthesize the CZTS nanostructure alloy. Copper (II) chloride dihydrate (0.6 M), zinc acetate (0.8 M), tin (II) chloride dihydrate (0.8 M), and thiourea (0.8 M) were dissolved individually in 10 ml of distilled (DI) water using a magnetic stirrer to prepare quaternary alloy precursor solutions. The prepared solutions were mixed in a 300-ml Pyrex beaker and stirred for 30 min at 70°C. At room temperature (30°C), droplets of sodium hydroxide were added to the solution mixture to maintain the pH at 12 and stirred until a gel was formed. The $Cu_2(Zn_{1-x}Mg_x)SnS_4$ alloy was synthesized by repeating the previous steps and adding 0.8 M magnesium chloride hexahydrate using stoichiometric ratios of each component, where $x = 0$ wt.%, 0.3 wt.%, 0.5 wt.%, 0.7wt.%, and 1 wt.%. The generated gel was washed with DI water and acetone to eliminate the sodium chloride and other traces found in the precipitate. A centrifugal separator was used to settle the precipitate, which was then filtered multiple times. Subsequently, the samples were dried for 40 h at 30°C before being annealed for 5 h at 800°C. All the chemicals and solvents were purchased from Sigma Aldrich (USA; 99.95%). The obtained powders were deposited on *n*-type silicon substrates using a sol–gel method, as reported by Ibraheam et al., [18] with a thickness of approximately 425 nm. Finally, Ag metal contacts were deposited on the thin-film samples using vacuum thermal evaporation (PVD-HANDY/2STE; USA) at 6×10^{-6} kPa. Zigzag-shaped contacts with a length of 5 mm and a thickness of 115 mm were employed to provide a surface contact area of approximately 3.14×10^2 cm^2, as illustrated in Fig. 1.

2.2 Analysis and Characterization

An x-ray diffractometer (XRD; Phillips, USA), with Cu Kα radiation with a wavelength of 1.54 Å, was used to investigate the structural properties of the $Cu_2(Zn_{1-x}Mg_x)SnS_4$ quaternary alloy. Photoluminescence (PL) spectroscopy (Jobin Yvon, USA) was used to analyze the quality of the developed films and determine the role of defects in the quaternary

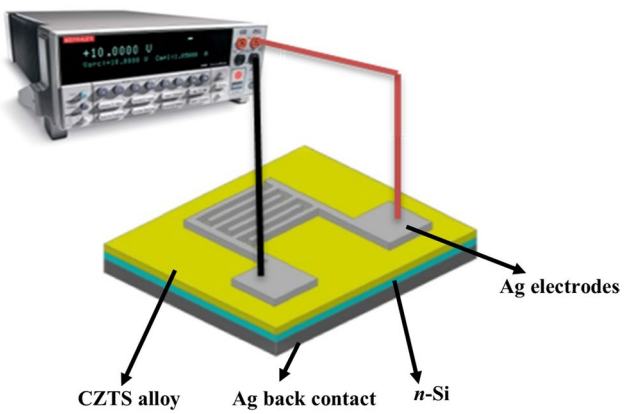

Fig. 1 Scheme of the *p–n* junction layer.

alloy. The surface morphologies of the prepared films were examined using field-emission scanning electron microscopy (FE-SEM; NOVA NANO SEM, USA). The source meter (Keithley 2400, USA) was coupled in parallel to the fabricated device for the *I–V* characterization, and it measured between −6 and 6 V. For current–time (*I–t*) analysis, the sample and multimeter were connected in series, and the current was measured by turning the LED on and off (415 nm wavelength, and 1640 mW output power).

3. Results and Discussion

The XRD patterns of the $Cu_2(Zn_{1-x}Mg_x)SnS_4$ films synthesized with various Mg wt.% (x) are illustrated in Fig. 2. At $x = 0$, the CZTS film exhibited the diffraction peaks (002), (101), and (200), assigned to the tetragonal kesterite phase (ICDD 01–075-4122), and (004), assigned to the stannite $CuMnSnS_4$ phase (at Mg = 1 wt.%) (ICDD 00–029-0537).[19] Additionally, the XRD profiles of the quaternary $Cu_2(Zn1_{-x}Mg_x)SnS_4$ nanostructure alloy showed no peaks belonging to other secondary phases, including those of MgS, ZnS, Cu_2S, and SnS, indicating that Mg was doped into the CZTS host lattice. The intensity of the (101) diffraction peak increased as the Mg content increased, demonstrating that the crystallinity of the quaternary alloy was enhanced. It would be interesting to investigate the degree of crystallinity (C_D) achieved with respect to the relevant structural parameters and to reveal the effect of Mg content on the obtained results. The C_D can be estimated using Eq. 1, which is the ratio of the integrated area of the crystalline peaks (Ac) to the total integrated area (Aa) under the XRD peaks.[20] The C_D as a function of the Mg content is displayed in Table I, based on the XRD measurements. One possible explanation for this finding is that the Mg content played an active role as a nucleation component in crystal growth.

$$C_D = \frac{A_c}{A_c + A_a} \times 100\% \tag{1}$$

The crystalline size (D) of the films was determined using Eq. 2 for the (101) peak using the Debye–Scherrer formula.[21] The D of the deposited films increased from 31.65 to 53.73 nm when the Mg wt.% increased from 0 to 1 wt.%, as reported in Table II. With increasing Mg wt.%, the decrease in the full width at half maximum (FWHM) resulted in a narrower dominant peak with higher intensities, indicating improved crystalline growth followed by an increase in D.[22] Hence, it can be concluded that the Mg content influences the crystallization size of CZTS.

$$D = \frac{k\lambda}{\beta\cos\theta}, \tag{2}$$

where λ is the wavelength of the CuKα line, β is the FWHM of the characteristic peak, and θ is the Bragg angle. The lattice parameters (a and c) of the (101) diffraction peak were calculated using[23]:

$$\frac{1}{d^2} = \frac{h^2 + k^2}{a^2} + \frac{l^2}{c^2} \tag{3}$$

As shown in Table II, when the Mg content increased, the (101) diffraction peak shifted to a lower diffraction angle, reflecting an increase in the lattice parameters of the $Cu_2(Zn_{1-x}Mg_x)SnS_4$ films. The increase in the lattice

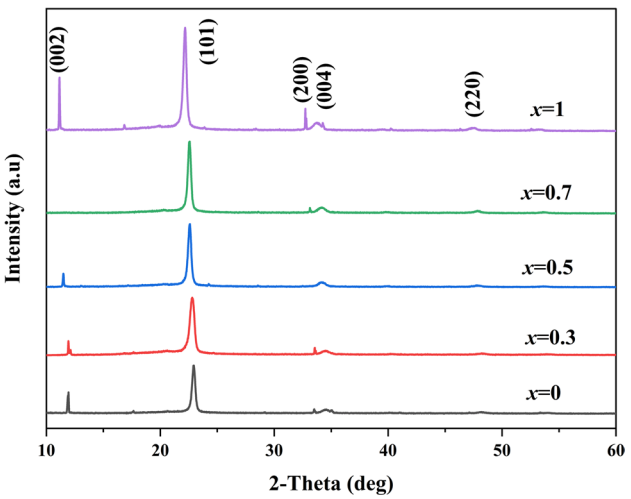

Fig. 2 XRD patterns of the $Cu_2(Zn_{1-x}Mg_x)SnS_4$ films synthesized with various Mg wt.% (x).

Table I Crystallinity of the $Cu_2(Zn_{1-x}Mg_x)SnS_4$ alloy with various Mg wt.% content

Mg wt.%	C_D%
0	49.08
0.3	54.18
0.5	57.55
0.7	63.34
1	69.23

Table II Structural parameters of $Cu_2(Zn_{1-x}Mg_x)SnS_4$ nanostructured thin film with various Mg wt.%

Mg wt.%	2θ (deg.)	D (nm)	Lattice parameters (Å)	
			a	c
0	22.92	31.65	5.428	10.857
0.3	22.78	36.58	5.446	10.864
0.5	22.58	40.25	5.549	10.882
0.7	22.51	44.27	5.556	11.201
1	22.21	53.73	5.573	11.415

parameters is attributed to the fact that the covalent radius of an Mg ion (1.36 Å) is larger than that of a Zn ion (1.25 Å). Consequently, this shows that the phase structure of the quaternary alloy did not change because the Zn ion sites were occupied by Mg in the host lattice of the quaternary alloy.[9,15,24] Furthermore, the substitution of Mg for other metals in the crystal lattice of the $Cu_2(Zn_{1-x}Mg_x)SnS_4$ alloy can also be explained using theoretical calculations of the local substitution energies of Mg with Cu, tin (Sn), and Zn. Because Mg–Zn has a lower substitution energy than Mg–Cu_2 and Mg–Sn_2, the Mg atoms substitute for the Zn atomic site, and this substitution does not affect the conduction type because Mg and Zn are isovalent.[17,25]

The quaternary $Cu_2(Zn_{1-x}Mg_x)SnS_4$ nanostructured alloy was elementally analyzed at different Mg contents using energy dispersive x-ray spectroscopy (EDX), and Fig. 3a–c. shows their compositions. The presence of Cu, Zn, Mg, Sn, and sulfide was confirmed by EDX. Table III summarizes the atomic content of the prepared samples; as the Zn atomic content decreased, the Mg atomic content gradually increased, demonstrating that Mg was incorporated into the $Cu_2(Zn_{1-x}Mg_x)SnS_4$ lattice, substituting Zn.[26] This result matches the findings that Mg replaces the Zn site based on the XRD analysis result.

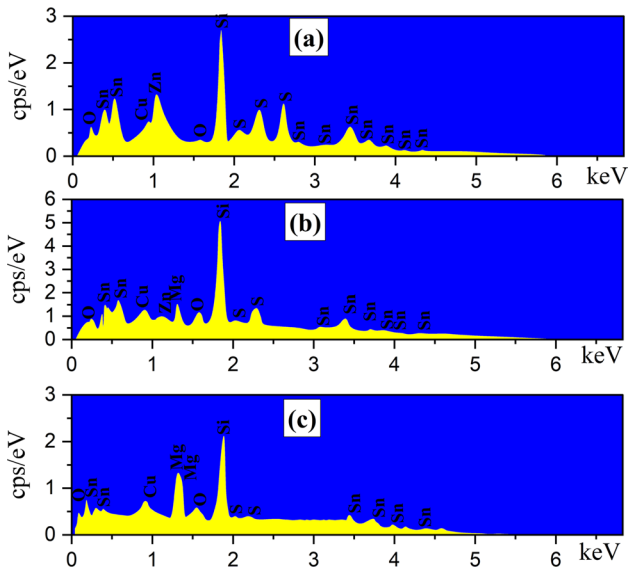

Fig. 3 EDX analysis of synthesized $Cu_2(Zn_{1-x}Mg_x)SnS_4$ quaternary alloy: (a) Mg wt.% = 0, (b) Mg wt.% = 0.7, and (c) Mg wt.% = 1.

FE-SEM images of the prepared $Cu_2(Zn1_{-x}Mg_x)SnS_4$ quaternary films with various Mg wt.% are shown in Fig. 4b–d. When the Mg content reached the maximum value (1 wt.%), the surface morphology changed from granular to whiskers, resulting in more densely packed nanostructures of less porosity. The structural quality of the $Cu_2(Zn_{1-x}Mg_x)SnS_4$ film morphology significantly improved, displaying the largest grain size with a dense and crack-free surface (Fig. 4e). The average grain size of the $Cu_2(Zn_{1-x}Mg_x)SnS_4$ films (Fig. 4f.) was estimated using ImageJ software. The absorber layer grain size influences the performance of photovoltaic devices; therefore, so larger grains are required to fabricate high solar cell efficiency.[9,19]

PL spectra with varying Mg content at room temperature are shown in Fig. 5. The emission peak positions shifted to higher wavelengths with increased peak intensity when the Mg content increased. Because the PL intensity is proportional to the number of photons released, the increased peak intensity indicates that more photons were released with increasing Mg content. The PL peak shifting can be explained by substituting the Zn atom with Mg, resulting in a decreased energy gap.[23] The shift in the position of the PL peaks can be explained by substituting the Zn atom with Mg, leading to an increase in the grain size and a subsequent reduction in the energy gap (E_g). The energy gap of the $Cu_2(Zn_{1-x}Mg_x)SnS_4$ samples with various Mg contents are listed in Table IV. The energy gap is calculated using:

$$E_g = \frac{1240}{\lambda} \tag{4}$$

where λ is the wavelength in nm.

The *I–V* characteristics of the CZTS and $Cu_2(Zn_{1-x}Mg_x)SnS_4$ thin films under LED illumination (I_{Light}) and in the dark (I_{Dark}) are shown in Fig. 6a–c. Figure 6 depicts the Ohmic behavior for the photocurrent, revealing an increase in photocurrent with an increase in applied voltage, as shown in Table V. The I_{Light} linear increase can be explained by an increase in forwarding bias voltage, which causes oxygen vacancies to move closer to the interface and increase the current.[27] Additionally, the increase in I_{Light} can be linked to the increase in the number of released photons induced by the Mg added content, as confirmed by the PL spectrum. In contrast, I_{Dark} decreased as Mg content increased. The decrease in I_{Dark} may be due to the enhanced crystalline characteristics, which reduce surface structural flaws, confirming the XRD findings and improving electrical attributes.[9,28]

Table III EDX composition analysis of $Cu_2(Zn_{1-x}Mg_x)SnS_4$ quaternary alloy nanostructured thin films

Mg content	Cu%	Mg%	Zn%	Sn%	O	S%
0	22.17	0	12.78	15.24	2.56	47.25
0.7	18.84	6.52	7.32	17.7	3.12	46.5
1	20.23	11.52	0	18.21	3.4	46.64

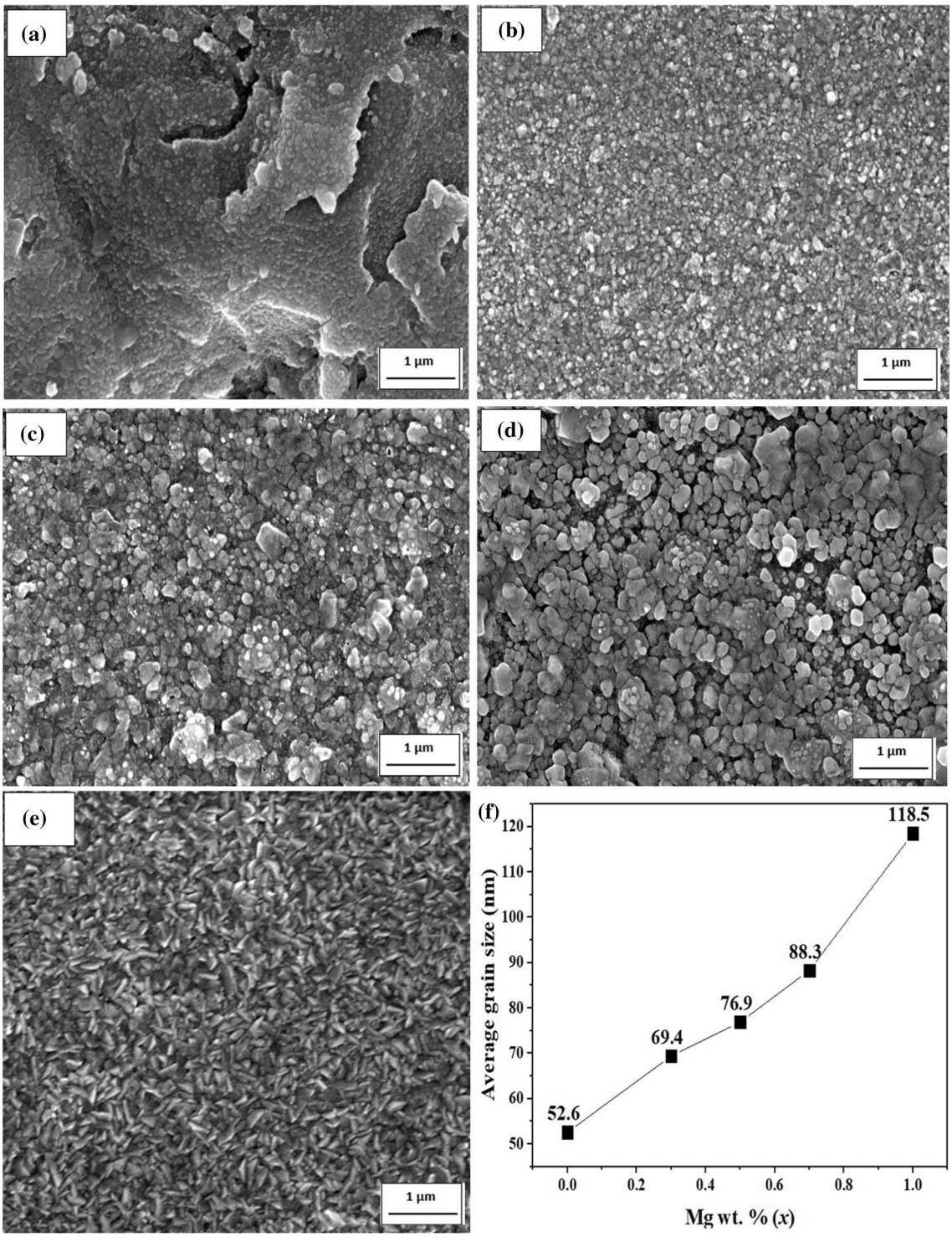

Fig. 4 FE-SEM images of $Cu_2(Zn_{1-x}Mg_x)SnS_4$ quaternary films with various Mg wt. % content (a-e) and (f) the average grain size versus Mg wt.%.

The photosensitivity (Ph_S%) of the tested samples was calculated at 6 V bias using Eq. 5 for the *I–V* characteristics,[29] and the I_{Light}, I_{Dark}, and Ph_S% results are included in Table VI. Ph_S% increased from 1888.24 to 5309.64% when the Mg contents increased to 0.7 wt.%, achieving maximum Ph_S% and supporting an improvement in absorber layer quality, whereas it decreased to 3520.25% when the Mg contents reached 1. The decrease in Ph_S% at 1 wt.%

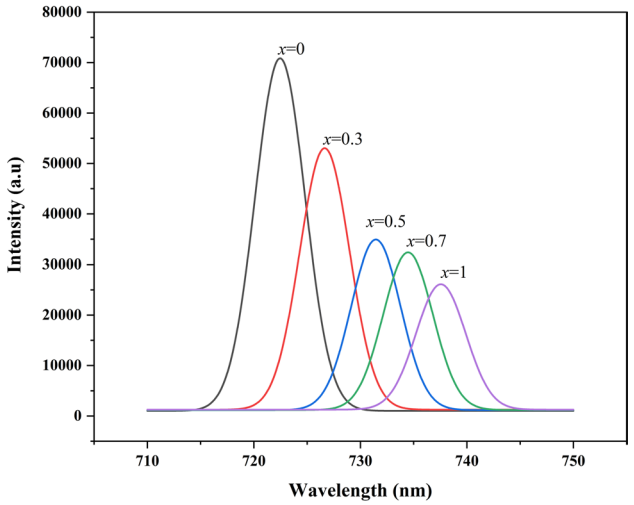

Fig. 5 PL spectra of $Cu_2(Zn_{1-x}Mg_x)SnS_4$ thin films with varying Mg wt.% (x) content.

Table IV Energy gap as a function of the Mg wt.% content

Mg content (X)	Energy gap (eV)
0	1.71
0.3	1.7
0.5	1.69
0.7	1.68
1	1.67

Mg may be attributed to an overall improvement in photovoltaic performance at 0.7 wt.% Mg content, which results in a reduction in I_{Light}, I_{Dark}, and Ph_S% at content larger than 0.7 wt.%:[9,28]

$$Ph_S = \frac{I_{Light} - I_{Dark}}{I_{Dark}} \times 100\% \quad (5)$$

The developed $Cu_2(Zn_{1-x}Mg_x)SnS_4$ films were tested to demonstrate their photocurrent responsivity (Ph_R%) and reproducibility by periodically turning the LED light on and off using Eq. (6).[18] Figure 7 displays the Ph_R% of the nanostructured quaternary alloy $Cu_2(Zn_{1-x}Mg_x)SnS_4$ as a function of time intervals (I–t) for Mg contents of 0, 0.7, and 1 wt.%. A sharp increase in the photocurrent was observed until it reaches a maximum (L_{on}) when the LED light was turned on and then decreased to a minimum (L_{off}) when the light is turned off. Table VII shows the response time (Res_t), decay time (Dec_t), and Ph_R% results:

$$Ph_R = \frac{L_{on} - L_{off}}{L_{on}} \times 100\% \quad (6)$$

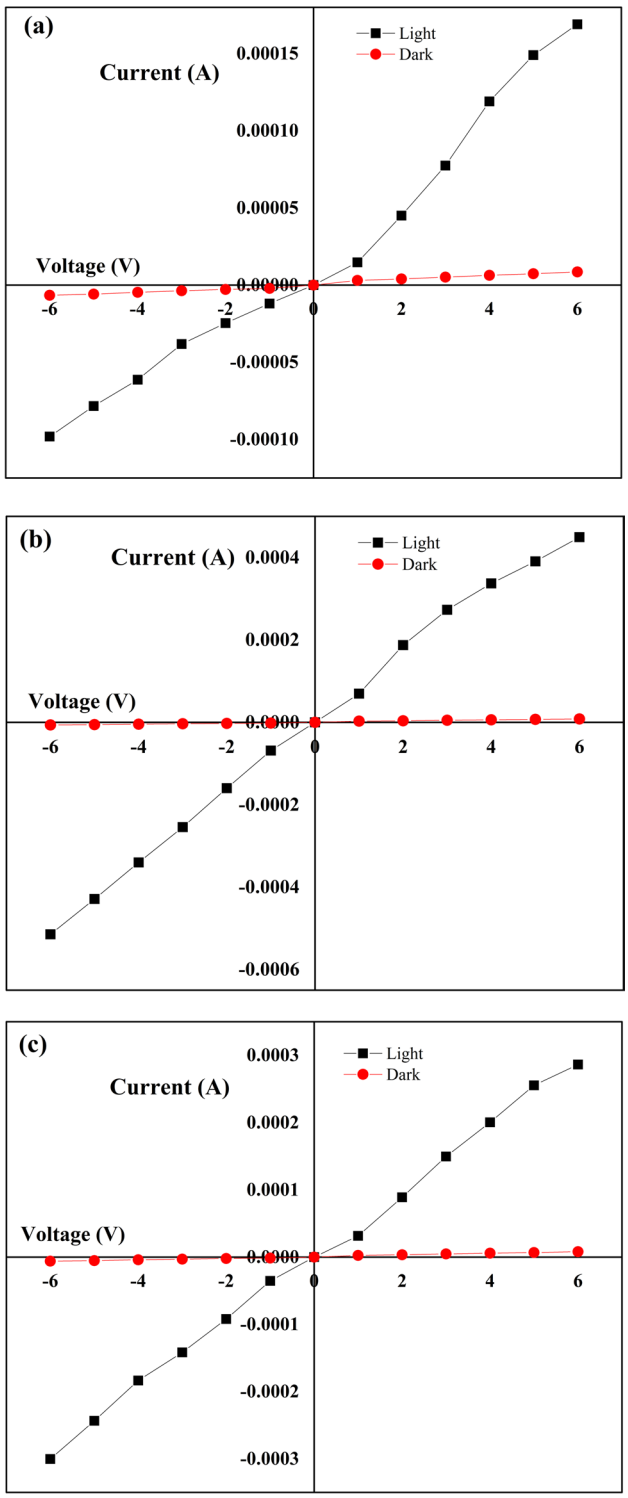

Fig. 6 I–V characteristics of (a) CZTS, (b) $Cu_2(Zn_{1-x}Mg_x)SnS_4$ with Mg wt. % = 0.7, and (c) $Cu_2(Zn_{1-x}Mg_x)SnS_4$ with Mg wt. % = 1. The samples were examined at 6 V bias under 490 nm LED light and in the dark.

Table V *I–V* characteristics of the CZTS and $Cu_2(Zn_{1-X}Mg_x)SnS_4$ thin films: (a) Mg wt. % = 0, (b) Mg wt. % = 0.7, ©) Mg wt. % = 1

Voltage (V)	Current (A)					
	(a)		(b)		(c)	
	$I_{Light} \times 10^{-4}$	$I_{Dark} \times 10^{-6}$	$I_{Light} \times 10^{-4}$	$I_{Dark} \times 10^{-6}$	$I_{Light} \times 10^{-4}$	$I_{Dark} \times 10^{-6}$
6	1.69	8.54	4.49	8.3	2.86	7.95
5	1.49	7.37	3.91	7.13	2.55	6.78
4	1.19	6.32	3.37	6.08	2	5.73
3	0.77	5.17	2.73	4.94	1.5	4.58
2	0.45	4.00	1.87	3.77	0.88	3.42
1	0.14	3.05	0.69	2.82	0.31	2.46
0	0	0	0	0	0	0
− 1	− 0.12	− 2.14	− 0.68	− 1.91	− 0.35	− 1.56
− 2	− 0.24	− 2.80	− 1.6	− 2.56	− 0.92	− 2.21
− 3	− 0.38	− 3.65	− 2.54	− 3.41	− 1.42	− 3.06
− 4	− 0.61	− 4.68	− 3.4	− 4.44	− 1.84	− 4.09
− 5	− 0.78	− 5.87	− 4.29	− 5.63	− 2.44	− 5.28
− 6	− 0.98	− 6.6	− 5.14	− 6.37	− 3	− 6.01

Table VI I_{Light}, I_{Dark}, I_{Light}-I_{Dark}, and Ph_S% results of $Cu_2(Zn_{1-x}Mg_x)SnS_4$ alloy with different Mg wt.%

Mg wt.%	$I_{light} \times 10^{-4}$ (A)	$I_{Dark} \times 10^{-6}$ (A)	$I_{light—}I_{dark} \times 10^{-4}$ (A)	Ph_S%
0	1.69	8.5	1.61	1888
0.7	4.49	8.3	4.41	5309
1	2.86	7.9	2.78	3520

Table VII Response time, decay time, and photocurrent responsivity of $Cu_2(Zn_{1-x}Mg_x)SnS_4$ alloy with different Mg wt.%.

Mg wt.% (*x*)	Res_t (s)	Dec_t (s)	Ph_R%
0	0.8743	0.2547	74
0.7	0.9152	0.3021	2319
1	0.9652	0.3578	791

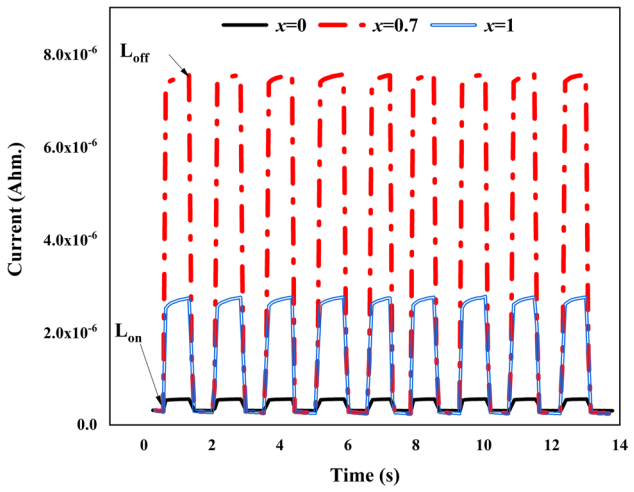

Fig. 7 Photocurrent responsivity of the $Cu_2Zn_{1-x}Mg_xSnS_4$ alloy under 490 nm LED light with various Mg wt.% (*x*) content.

The Ph_R% findings revealed increased sensitivity when the Mg content was introduced. The sample with Mg content of 0.7 wt.% achieved the highest sensitivity (2319%) with a faster response/recovery time of approximately 0.9152 s/0.3021 s, as reported in Table VII.

4. Conclusions

Nanostructured $Cu_2(Zn_{1-x}Mg_x)SnS_4$ quaternary alloy was successfully deposited on a silicon substrate using an environmentally friendly method. The current study showed that the Mg content improved the structural, morphological, and electrical properties of the deposited quaternary alloy thin film. Structural analysis of the $Cu_2(Zn_{1-x}Mg_x)SnS_4$ films indicated that the Mg concentration affected *D* and improved the electrical characteristics. Furthermore, as the Mg content increased, the morphology significantly improved, resulting in a larger particle size. Finally, the Mg content of the $Cu_2(Zn_{1-x}Mg_x)SnS_4$ alloy improved the ultraviolet light-absorbing layer. In general, the Mg content enhanced the sensitivity of the CZTS quaternary alloy to ultraviolet light, and the sample containing 0.7 wt.% Mg attained around 31% higher Ph_R% than the as-deposited CZTS quaternary alloy, indicating that the developed quaternary alloys are adequate for ultraviolet light detection.

Acknowledgements We would like to thank Editage (www.editage.com) for English language editing.

Conflict of interest The authors declare that they have no known conflicting financial interests or personal relationships that could have appeared to influence the work reported in this paper.

References

1. Y. Du, S. Wang, Q. Tian, Y. Zhao, X. Chang, H. Xiao, Y. Deng, S. Chen, S. Wu, and S. Liu, Defect Engineering in Earth-Abundant $Cu_2ZnSn(S, Se)_4$ Photovoltaic Materials via Ga^{3+} -Doping for over 12% Efficient Solar Cells. *Adv. Funct. Mater.* **31**, 2010325 (2021).
2. A.S. Ibraheam, Y. Al-Douri, U. Hashim, M.R. Ghezzar, A. Addou, and W.K. Ahmed, Cadmium Effect on Optical Properties of $Cu_2Zn_{1-x}Cd_xSnS_4$ Quinternary Alloys Nanostructures. *Sol. Energy* **114**, 39 (2015).
3. Z. Liu and X. Su, A Novel Fluorescent DNA Sensor for Ultrasensitive Detection Of Helicobacter Pylori. *Biosens. Bioelectron.* **87**, 66 (2017).
4. P. Jackson, R. Wuerz, D. Hariskos, E. Lotter, W. Witte, and M. Powalla Effects of heavy alkali elements in $Cu(In,Ga)Se_2$ solar cells with efficiencies up to 22.6%. *Phys. Status Solidi – Rapid Res. Lett.* **10**, 583 (2016).
5. T. Gokmen, O. Gunawan, T.K. Todorov, and D.B. Mitzi, Band Tailing and Efficiency Limitation in Kesterite Solar Cells. *Appl. Phys. Lett.* **103**, 103506 (2013).
6. S.K. Wallace, D.B. Mitzi, and A. Walsh, The Steady Rise of Kesterite Solar Cells. *ACS Energy Lett.* **2**, 776 (2017).
7. W. Bao and F.-Y. Sachuronggui, Band Offsets Engineering at Cd_xZn_1-xS/Cu_2ZnSnS_4 Heterointerface. *Chin. Phys. B* **25**, 127102 (2016). https://doi.org/10.1088/1674-1056/25/12/127102.
8. D. Shin, B. Saparov, and D.B. Mitzi, Defect Engineering in Multinary Earth-Abundant Chalcogenide Photovoltaic Materials. *Adv. Energy Mater.* **7**, 1602366 (2017).
9. S. Lie, S.W. Leow, D.M. Bishop, M. Guc, V. Izquierdo-Roca, O. Gunawan, and L.H. Wong, Improving Carrier-Transport Properties of CZTS by Mg Incorporation with Spray Pyrolysis. *ACS Appl. Mater. Interfaces* **11**, 25824 (2019).
10. L. Choubrac, A. Lafond, M. Paris, C. Guillot-Deudon, and S. Jobic, The Stability Domain of the Selenide Kesterite Photovoltaic Materials and NMR Investigation of the Cu/Zn Disorder in $Cu_2ZnSnSe_4$ (CZTSe). *Phys. Chem. Chem. Phys.* **17**, 15088 (2015).
11. S. Lie, J.M.R. Tan, W. Li, S.W. Leow, Y.F. Tay, D.M. Bishop, O. Gunawan, and L.H. Wong, Reducing the Interfacial Defect Density of CZTSSe Solar Cells by Mn Substitution. *J Mater Chem. A* **6**, 1540–1550 (2018). https://doi.org/10.1039/C7TA09668B.
12. M. Souli, R. Engazou, L. Ajili, and N. Kamoun-Turki, Physical Properties Evolution of Sprayed Cu_2MgSnS_4 Thin Films with Growth Parameters and Vacuum Annealing. *Superlattices Microstruct.* **147**, 106711 (2020).
13. A. Ali, Y. Liang, S. Ahmed, B. Yang, B. Guo, and Y. Yang, Mutual Contaminants Relational Realization and Photocatalytic Treatment Using Cu_2MgSnS_4 Decorated $BaTiO_3$. *Appl. Mater. Today* **18**, 100534 (2020).
14. M. Wei, Q. Du, R. Wang, G. Jiang, W. Liu, and C. Zhu, Synthesis of New Earth-abundant Kesterite Cu_2MgSnS_4 Nanoparticles by Hot-injection Method. *Chem. Lett.* **43**, 1149 (2014).
15. Y. Zhang, D. Jiang, Y. Sui, Y. Wu, Z. Wang, L. Yang, F. Wang, S. Lv, and B. Yao, Synthesis and Investigation Of Environmental Protection and Earth-Abundant Kesterite $Cu_2Mg_xZn_{1-x}Sn(S, Se)_4$ Thin Films for Solar Cells. *Ceram. Int.* **44**, 15249 (2018).
16. Y. Wang, Y. Yang, C. Zhu, H. Luan, R. Liu, L. Wang, C. Zhao, and X. Lv, Boosting the Electrical Properties of $Cu_2ZnSn(S, Se)_4$ Solar Cells via Low Amounts of Mg Substituting Zn. *ACS Appl. Energy Mater.* **3**, 11177 (2020).
17. D.M. Mena, D.V. Romero, C.L. Valenzuela, and A. Ricardo, Partial and Total Substitution of Zn by Mg in the Cu_2ZnSnS_4 Structure. *Curr. Comput.-Aided Drug Des.* **10**, 578 (2020). https://doi.org/10.3390/cryst10070578.
18. A.S. Ibraheam, Y. Al-Douri, U. Hashim, M. Ameri, A. Bouhemadou, and R. Khenata, Structural, Optical and Electrical Investigations of $Cu_2Zn_{1-x}Cd_xSnS_4$/Si Quinternary Alloy Nanostructures Synthesized by Spin Coating Technique. *Microsyst. Technol.* **23**, 2223 (2017).
19. A. Bhattacharya, D.G. Tkachuk, A. Mar, and V.K. Michaelis, Mere Anarchy is Loosed: Structural Disorder in $Cu_2Zn_{1-x}Cd_xSnS_4$. *Chem. Mater.* **33**, 4709 (2021).
20. M. Doumeng, L. Makhlouf, F. Berthet, O. Marsan, K. Delbé, J. Denape, and F. Chabert, A Comparative Study of the Crystallinity of Polyetheretherketone by using density, DSC, XRD, and Raman Spectroscopy Techniques. *Polym. Test.* **93**, 106878 (2021).
21. A.A. Khalefa, J.M. Marei, H.A. Radwan, and J.M. Rzaij, In_2O_3-CuO NANO-Flakes Prepared By Spray Pyrolysis for Gas Sensing Application. *Dig. J. Nanomater. Biostructures* **16**, 197 (2021).
22. J.M. Rzaij, A.S. Ibraheam, and A.M. Abass, Cobalt Effect on the Growth of Cadmium Oxide Nanostructure Prepared by Spray Pyrolysis Technique. *Baghdad Sci. J.* **18**, 401 (2021).
23. Q.A. Abduljabbar, H.A. Radwan, J.M. Marei, and J.M. Rzaij, Spray Rate Effects on the NO_2 Gas Sensor Properties of Ni-doped SnO_2 Nanoflakes. *Eng. Res. Express* **4**, 015028 (2022).
24. G.L. Agawane, S.A. Vanalakar, A.S. Kamble, A.V. Moholkar, and J.H. Kim, Fabrication of $Cu_2(Zn_xMg_{1-x})SnS_4$ Thin Films by Pulsed Laser Deposition Technique for Solar Cell Applications. *Mater. Sci. Semicond. Process.* **76**, 50 (2018).
25. D. Sun, Y. Ding, L. Kong, Y. Zhang, X. Guo, L. Wei, L. Zhang, and L. Zhang, First-principles Study on Mg Doping in Cu_2ZnSnS_4. *J. Inorg. Mater.* **35**, 1290 (2020).
26. Y. Sui, Y. Zhang, D. Jiang, W. He, Z. Wang, F. Wang, B. Yao, and L. Yang, Investigation of Optimum Mg Doping Content and Annealing Parameters of $Cu_2Mg_xZn_{1-x}SnS_4$ Thin Films for Solar Cells. *Nanomaterials* **9**, 955 (2019).
27. R. Chen and C. Persson, Electronic and Optical Properties of Cu_2XSnS_4 (X = Be, Mg, Ca, Mn, Fe, and Ni) and the Impact of Native Defect Pairs. *J. Appl. Phys.* **121**, 203104 (2017).
28. K.F. Tse, S. Wang, M.H. Wong, and J. Zhu, Defects Properties and Vacancy Diffusion in Cu_2MgSnS_4. *J. Semicond.* **43**, 022101 (2022).
29. A.S. Ibraheam, J.M. Rzaij, and M.A. Fakhri, Structural, Optical and Electrical Investigations of Al:ZnO Nanostructures as UV Photodetector Synthesized by Spray Pyrolysis Technique. *Mater. Res. Express* **6**, 055916 (2019).